Journal of Hazardous Materials 219–220 (2012) 276–282

Contents lists available at SciVerse ScienceDirect

Journal of Hazardous Materials

journal homepage: www.elsevier.com/locate/jhazmat

Enhanced electron transfer and silver-releasing suppression in Ag–AgBr/titanium-doped Al_2O_3 suspensions with visible-light irradiation

Xuefeng Zhou, Chun Hu*, Xuexiang Hu, Tianwei Peng

State Key Laboratory of Environmental Aquatic Chemistry, Research Center for Eco-Environmental Sciences, Chinese Academy of Sciences, Beijing 100085, China

ARTICLE INFO

Article history:
Received 12 November 2011
Received in revised form 2 April 2012
Accepted 3 April 2012
Available online 10 April 2012

Keywords:
Ag–AgBr/Ti-doped mesoporous alumina
Plasmon-assisted photocatalyst
Ag dissolution
Charge transfer
Photoactivity

ABSTRACT

Ag–AgBr was deposited onto mesoporous alumina (MA) and titanium-doped MA by a deposition–precipitation method. The photocatalytic activity and the dissolution of Ag^+ from different catalysts were investigated during the photodegradation of 2-chlorophenol (2-CP) and phenol in ultrapure water and tap water with visible-light irradiation. With the increase in doped titanium, the Ag^+ dissolution decreased with a decrease in the photocatalytic activity. Ag–AgBr/MA-Ti1 was considered the better catalyst for practical applications because its Ag^+ dissolution was minimal (0.4 mg L^{-1} in ultrapure water and 5 μg L^{-1} in tap water), although its photoactivity was slightly less than that of Ag–AgBr/MA. The dissolution of Ag^+ was related to a charge–transfer process based on the study of cyclic voltammetry analyses under a variety of experimental conditions. The results suggested that several types of anions in the water, including CO_3^{2-}, SO_4^{2-}, and Cl^-, could act as electron donors that trap the photogenerated holes on Ag nanoparticles to facilitate electron circulation; this would decrease the release of Ag^+. Our studies indicated that the catalyst had a higher activity and stability in water purification.

1. Introduction

Semiconductor–metal nanocomposites have been widely employed in photocatalysis and are considered a cost-effective alternative for the destruction of persistent toxic organic compounds [1]. Various metals and semiconductors are used to synthesize semiconductor–metal photocatalysts, such as gold (Au) or silver (Ag) deposited on TiO_2 or ZrO_2 [2–4]. The metal in contact with the semiconductor greatly enhances the overall photocatalytic efficiency. The role the metal plays in the interfacial charge–transfer processes is not yet fully understood. The electron transfer between photoexcited semiconductors and metals is considered an important phenomenon in photocatalysis. Earlier investigations on semiconductor–metal composites revealed that the deposition of metal onto a semiconductor enhanced the efficiency of the photocatalytic redox processes [5–7]. Beside this, noble metal NPs such as Ag and Au exhibit strong UV–vis absorption due to their plasmon resonance [8,9], which is produced by the collective oscillations of the surface electrons. In particular, Au and Ag have attracted more attention because of their absorption properties in the visible region due to plasmon resonance [10–13]. Based on these properties, noble metal NPs have been used as photocatalysts and photovoltaic cell materials [14,15]. For most metal NPs dispersed on an oxide surface or other support catalyst, the electron transfer was based on both photoexcitation and plasmon-excitation of the surface [16,17]. The catalyst structure resulted in exposing the metals to the reactants and the surrounding medium [18]. Corrosion and dissolution of the metal NPs during the photocatalytic reaction tends to limit the use of metal NPs, especially for those such as Ag and Au. Recently, we reported that Ag–AgBr NPs were highly dispersed on the surface of ordered mesoporous γ-Al_2O_3, which exhibited high photocatalytic activity for the degradation and mineralization of toxic persistent organic pollutants [19]. This was due to the Ag NPs plasmon-assisted effect on the AgBr photocatalyst. Moreover, two plasmon-induced electron-transfer processes were verified: the transfer from the excited Ag NPs to AgBr, and the transfer from the pollutants to the Ag NPs. These processes produced $O_2^{\bullet -}$ and photogenerated holes (h^+) on the Ag NPs.

The high photocatalytic activity and photostability of the Ag halides have been attributed to the electron transfer induced by the plasmon resonance of Ag NPs on the surface of Ag halides [20–22]. However, the application of the photocatalyst was limited by the dissolution of Ag^+. To address these limitations, Ag–AgBr NPs were deposited on ordered mesoporous γ-Al_2O_3 (MA) and titanium-doped MA to reduce the dissolution of Ag^+ in the photoreaction. Phenol and 2-chlorophenol (2-CP), two ubiquitous water pollutants, were selected to evaluate the activity and Ag^+ dissolution of the catalysts under visible-light illumination. A photoinduced metal-dissolving mechanism was verified by cyclic voltammetry (CV) analyses under a variety of experimental conditions, which provided insight into improving these photocatalysts for practical applications.

* Corresponding author. Tel.: +86 10 62849628; fax: +86 10 62923541.
E-mail address: huchun@rcees.ac.cn (C. Hu).

0304-3894/$ – see front matter © 2012 Published by Elsevier B.V.
http://dx.doi.org/10.1016/j.jhazmat.2012.04.009

2. Experimental

2.1. Chemicals and materials

The reagent $(PEO)_{20}$–$(PPO)_{70}$–$(PEO)_{20}$ (Pluronic P123) was purchased from Sigma Chemical Company. All other chemicals used were analytical grade, purchased from the Beijing Chemical Company and used without further purification.

2.2. Preparation of catalysts

Mesoporous γ-Al_2O_3 was prepared from precursors of aluminum i-propoxide in the presence of glucose in an aqueous system as described previously [23,24]. Titanium was doped into MA during its synthesis process. Then 1% $Ti(SO_4)_2$ (0.05 g) and 5% $Ti(SO_4)_2$ (0.25 g) were dissolved in 30 mL of H_2O, which was then added to the suspension of mixed glucose (3.6 g) and alumina i-propoxide (4.2 g), respectively. The solutions were then calcined in air at 873 K for 6 h. Ag–AgBr was then deposited onto MA, MA-Ti1, and MA-Ti5, respectively, using the deposition–precipitation method as reported in our previous work [19].

2.3. Characterization

The samples were examined by obtaining X-ray diffraction (XRD) patterns (XDS-2000 diffractometer; Scintag Inc.) and UV–vis diffuse reflection spectra (Hitachi UV-3100). The high-resolution transmission electron microscopy (HRTEM) images were obtained by using a JEOL-2010 TEM with an acceleration voltage of 200 kV. X-ray photoelectron spectroscopy (XPS) and Auger electron spectroscopy (AES) data were taken on a PHI Quantera SXM spectrometer using monochromatic Al Kα radiation and low-energy electron-flooding for charge compensation. All binding energies were calibrated by the C 1s hydrocarbon peak at 284.80 eV. The photocurrents from the various samples were measured in a basic electrochemical system (AMETEK Princeton Applied Research) with a two compartment, three-electrode electrochemical cell equipped with a photocatalyst photoanode (prepared by dip-coating and drying in air at 70 °C) and a platinum wire cathode in a 0.1 M Na_2SO_4 solution. The reference electrode was a saturated calomel electrode.

2.4. Photocatalytic degradation of chlorophenolic compounds under visible light

Photocatalytic experiments were performed in a breaker with an aqueous suspension of phenolic pollutants (60 mL, 10 mg L^{-1}) and l00 mg of catalyst powder. The 350 W Xe-arc lamp light source, equipped with wavelength cutoff filters for λ > 420 nm, was focused onto the breaker. The concentration of each phenolic pollutant was measured using high-performance liquid chromatography with an eclipse XDB-C18 column (5 μm, 4.6 mm × 150 mm; Agilent). The concentration of Ag^+ dissolved in the photoreaction was measured by inductively coupled plasma-optical-emission spectrometry (ICP-OES) on an OPTIMA 2000 (Perkin-Elmer) instrument.

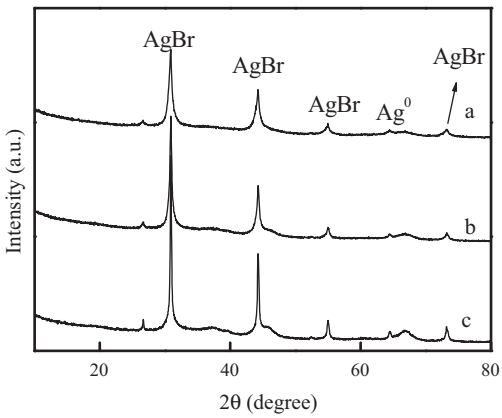

Fig. 1. XRD pattern of: (a) Ag–AgBr/MA, (b) Ag–AgBr/MA-Ti1, and (c) Ag–AgBr/MA-Ti5.

3. Results and discussion

3.1. Characterization of catalysts

Fig. 1 shows the XRD pattern of different samples. The diffraction peaks of Ag (JCPDS 65-2871) and AgBr (JCPDS 06-0438) were observed in all samples. The intensities of the XRD diffraction peaks of Ag–AgBr/MA were much less than those of Ag–AgBr supported on titanium-doped MA. With an increasing amount of titanium in MA, the intensities of the peaks increased, indicating an increase in the size of the Ag–AgBr crystallites in titanium-doped MA.

Fig. 2 showed HRTEM images of these samples. Ag–AgBr NPs were uniformly dispersed on the surfaces of MA, MA-Ti1, and MA-Ti5 for these catalysts. Their crystalline sizes were in the range of 10–20 nm, and the shape was a regular cubic structure. The Ag–AgBr NPs on MA-Ti1 and MA-Ti5 were aggregated and the crystalline size was slightly bigger than that in Ag–AgBr/MA. The results were in agreement with the results from XRD. As shown in Fig. 3A, for Ag–AgBr/MA-Ti1, the binding energies (BE) of Ti $2p_{3/2}$ and Ti $2p_{1/2}$ were 458.8 eV and 464.6 eV, respectively; this coincided with Ti^{4+}, indicating that titanium existed as Ti^{4+} in MA-Ti1. Fig. 3B showed the AES spectrum of the Ag element in the catalyst. The Auger peaks of silver were observed for Ag^0 at 1130.4 eV and Ag^+

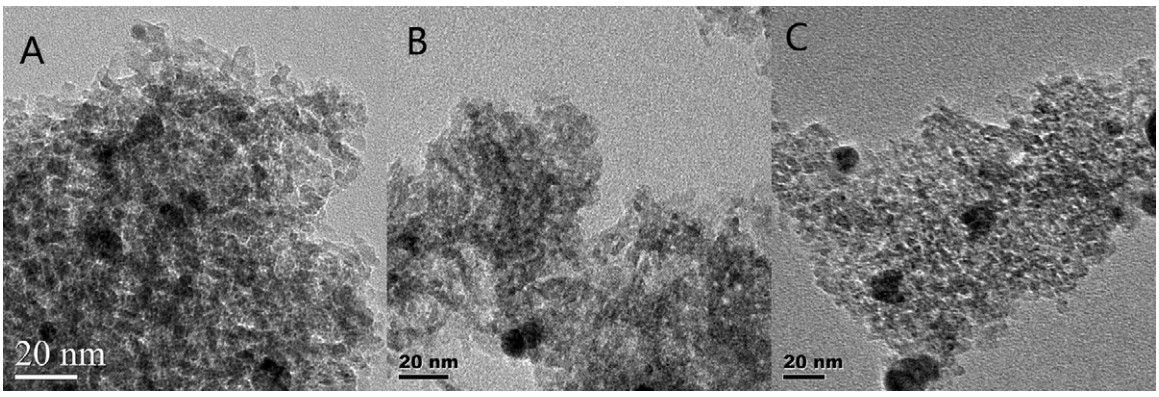

Fig. 2. Representative HRTEM images of: (A) Ag–AgBr/MA, (B) Ag–AgBr/MA-Ti1, and (C) Ag–AgBr/MA-Ti5.

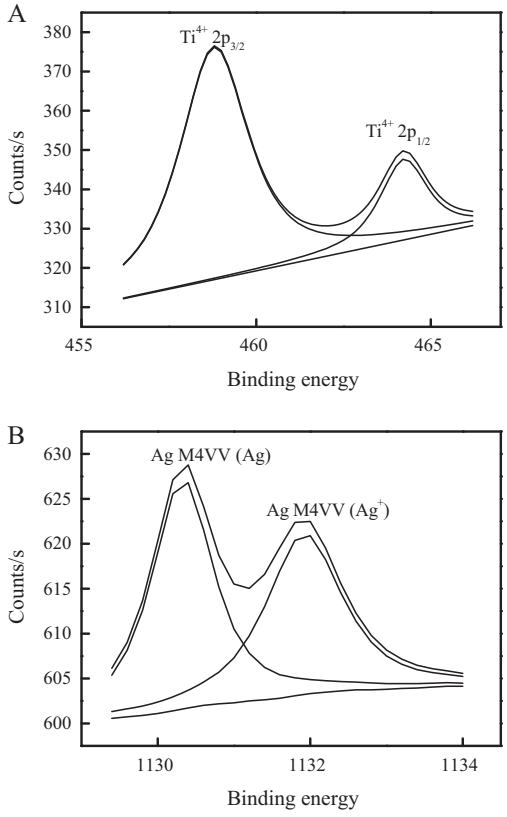

Fig. 3. Ti 2p XPS spectra (A) and Ag AES spectra (B) for AgBr/MA-Ti1.

at 1131.9 eV [22]. On the basis of the peak areas, the surface Ag^0 and Ag^+ contents were individually calculated to be 5.2% and 6.1%, respectively.

The relative UV–vis absorption spectra of Ag–AgBr on different supports varied as shown in the insets of Fig. 4. The Ag–AgBr on MA had a much stronger UV absorption than the others, indicating that Ag–AgBr NPs of greater size were formed on the titanium-doped MA, which was in good agreement with the results from the XRD patterns. A visible absorption band around 400–700 nm was also observed for all of the samples and assigned to the mixed peaks of AgBr NP absorption and the plasmon resonance of the Ag NPs. Subsequently, these spectra were converted into Kubelka–Munk functions and deconvoluted into Gaussian subbands that could be assigned to different Ag species [25]. The deconvolution was carried out based on the relative intensities of these subbands and the corresponding percentages of the different Ag species were obtained [26,27]. The band at 228 nm was attributable to the highly dispersed Ag^+ ions. The bands in the range of 297–303 nm were assigned to small $Ag_n^{\delta+}$ clusters. The bands between 400 nm and 600 nm were attributed to Ag NPs of various sizes. Thus, the contents of Ag^0 NPs on Ag–AgBr/MA, Ag–AgBr/MA-Ti1, and Ag–AgBr/MA-Ti5 were approximately 2.1%, 3.8%, and 4.6%, respectively. The bands near 398 nm and 532 nm were assigned to the Ag^0 NPs on Ag–AgBr/MA and Ag–AgBr/MA-Ti1, while the bands around 410 nm and 574 nm were attributable to the Ag^0 NPs on Ag–AgBr/MA-Ti5. The plasmon resonance of Ag NPs increased as the size of the particles increased. The contents of the dispersed Ag^+ ions were 0.34%, 0.22%, and 0.3%, and those of $Ag_n^{\delta+}$ clusters were 7.52%, 5.96%, and 5.15%, respectively. The BET surface areas were 287, 253, and 231 $m^2\ g^{-1}$ for MA, MA-Ti1, and MA-Ti5, respectively, indicating that the increase of the amount of doped titanium on MA decreased the surface area of MA, leading to bigger particle size, and lower dispersion of the Ag^0 NPs on the surface of MA-doped with titanium.

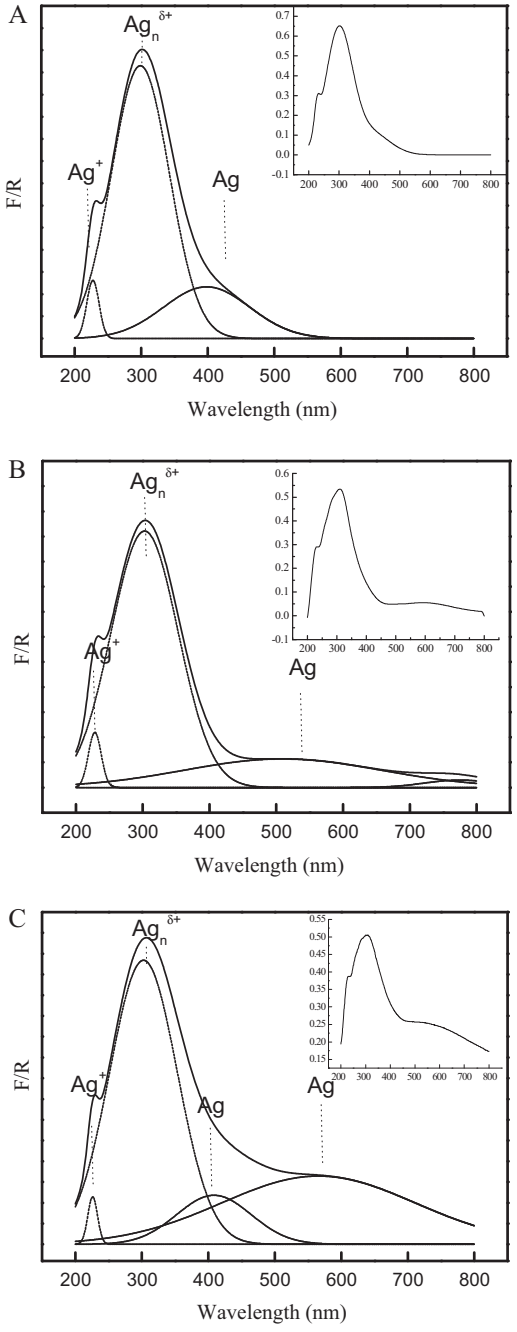

Fig. 4. Deconvoluted subbands of Ag–AgBr/MA (A), Ag–AgBr/MA-Ti1 (B), and Ag–AgBr/MA-Ti5 (C). Insets represent the relative UV–vis absorption spectra of the catalysts.

3.2. Photoactivity and photodissolution of Ag^+ for catalysts

To evaluate the photocatalytic activity of Ag–AgBr deposited on MA-doped with titanium, the photodegradation of 2-CP was carried out in an aqueous dispersion under visible-light irradiation. This photodegradation process occurred after the adsorption of 2-CP on the catalyst had reached equilibrium in the dark (Fig. 5). 2-CP was completely photodegraded within 25 min in the Ag–AgBr/MA suspension while the same results were obtained within 30 min in the Ag–AgBr/MA-Ti1 and Ag–AgBr/MA-Ti5 suspensions. The results indicated that Ag–AgBr deposited onto MA showed greater activity than Ag–AgBr deposited onto MA doped with titanium due to its higher dispersion on MA.

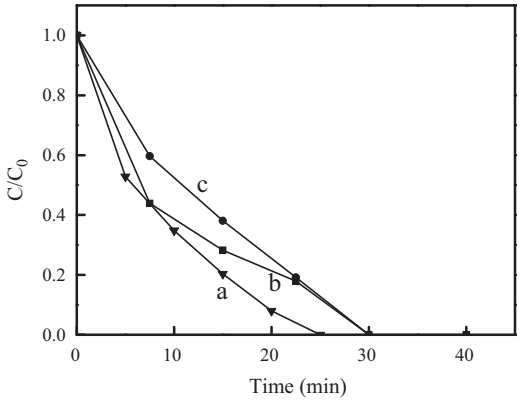

Fig. 5. Photodegradation of 2-CP (10 mg L^{-1}; 60 mL) aqueous dispersions (containing catalyst: 1.6 g L^{-1}) under visible light ($\lambda > 420$ nm): (a) Ag–AgBr/MA, (b) Ag–AgBr/MA-Ti1, and (c) Ag–AgBr/MA-Ti5.

Correspondingly, the Ag^+ dissolution from different catalysts was examined during the photodegradation of 2-CP in ultrapure water under visible light ($\lambda > 420$ nm). As shown in Fig. 6, the maximum concentration of Ag^+ dissolved from Ag–AgBr/MA was observed while the Ag^+ release was greatly inhibited in Ag–AgBr/MA-Ti1 and Ag–AgBr/MA-Ti5 suspensions. With increasing reaction time, the concentration of Ag^+ in solution decreased in the three reactions, indicating that the dissolved Ag^+ was photoreduced onto the surface of the catalysts again. Cl^- was formed with the degradation of 2-CP; however, this could potentially lower the concentration of Ag^+ by the precipitation of AgCl. For this reason, phenol was selected to investigate the Ag^+ dissolution under otherwise identical conditions (Fig. 7). The photoactivity of the different catalysts and the Ag^+ release during the degradation of phenol paralleled those in the degradation of 2-CP. The photocatalytic activity of these catalysts did not change significantly for the photodegradation of phenol in ultrapure and tap water. Moreover, the Ag–AgBr/MA-Ti1 exhibited better stability for five successive cycles of degradation testing under visible-light irradiation (Fig. 8). As shown in Fig. 9A, the Ag^+ release tended to zero after 50 min of reaction in Ag–AgBr/MA-Ti1 and AgBr/MA-Ti5 suspensions in ultrapure water, while the concentration of Ag^+ in the Ag–AgBr/MA suspension was around 3 mg L^{-1}. In contrast, in tap water, the Ag^+ release was greatly suppressed in the three catalyst suspensions, ranging from 70 to 10 μg L^{-1} (Fig. 9B). The concentration of Ag^+ dissolved from Ag–AgBr/MA-Ti1 and Ag–AgBr/MA-Ti5 ranged from 20 to 5 μg L^{-1} and 8 to 0 μg L^{-1}, respectively, while the concentration of Ag^+ dissolved from Ag–AgBr/MA varied from 70 to 10 μg L^{-1},

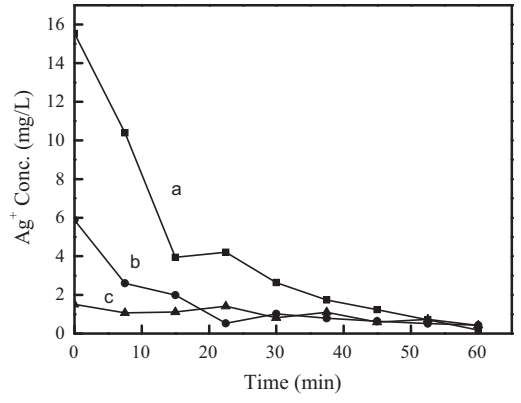

Fig. 6. The Ag^+ dissolution during the photodegradation of 2-CP (10 mg L^{-1}; 60 mL) in aqueous dispersion (containing catalyst: 1.6 g L^{-1}) under visible light ($\lambda > 420$ nm): (a) Ag–AgBr/MA, (b) Ag–AgBr/MA-Ti1, and (c) Ag–AgBr/MA-Ti5.

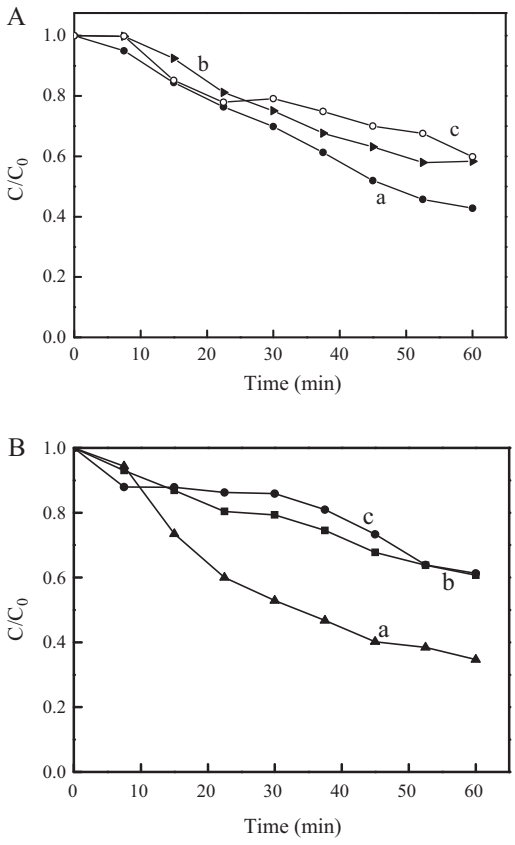

Fig. 7. The photodegradation of phenol (10 mg L^{-1}; 60 mL) in ultrapure (A) and tap water (B) solution dispersions (containing catalyst: 1.6 g L^{-1}) under visible light ($\lambda > 420$ nm): (a) Ag–AgBr/MA, (b) Ag–AgBr/MA-Ti1, and (c) Ag–AgBr/MA-Ti5.

indicating that donors in the tap water possibly reduced the photogenerated Ag^+ on the Ag NPs to decrease the dissolution of Ag NPs [28]. Compared with Figs. 6 and 9, the released Ag^+ concentration in the Ag–AgBr/MA suspension was much higher than that in Ag–AgBr/MA-Ti1 and Ag–AgBr/MA-Ti5 suspensions before irradiation. The results were attributable to the oxidization of Ag NPs by O_2 in the aqueous solution [17], which has been observed by CV analysis. The smaller particle size of the Ag NPs led to a higher activity of Ag NPs reacting with O_2. The resulting increase in the Ag^+ release led to higher photoactivity under irradiation [19]. As a whole, the results revealed that Ag–AgBr/MA-Ti1 was a better catalyst due to its stability and high photoactivity, although its photoactivity

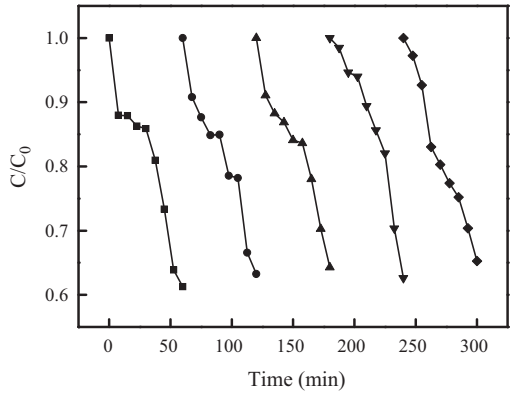

Fig. 8. Cycling runs in the photodegradation of phenol (10 mg L^{-1}; 60 mL) in Ag–AgBr/MA-Ti1 aqueous dispersion under visible light ($\lambda > 420$ nm).

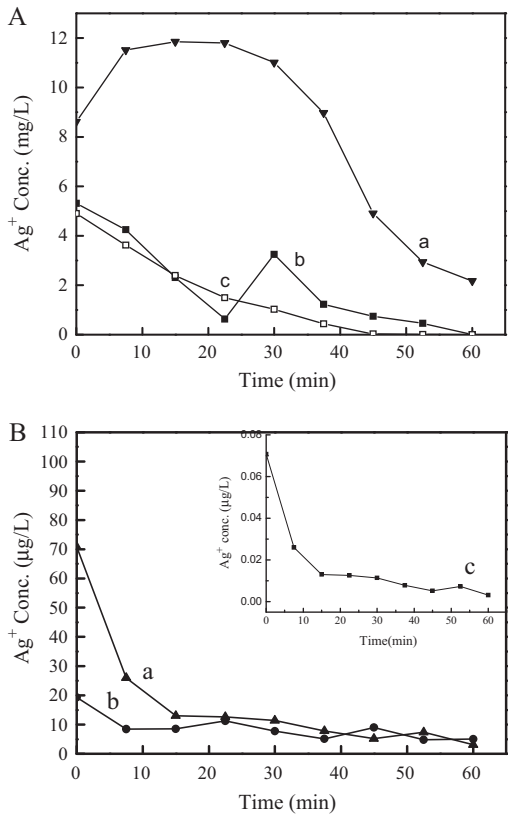

Fig. 9. The Ag^+ dissolution during the photodegradation of phenol (10 mg L^{-1}; 60 mL) in ultrapure (A) and tap water (B) solution dispersions (containing catalyst: 1.6 g L^{-1}) under visible light ($\lambda > 420$ nm): (a) Ag–AgBr/MA, (b) Ag–AgBr/MA-Ti1, and (c) Ag–AgBr/MA-Ti5 (in the inset of B).

was slightly lower than Ag–AgBr/MA for the photodegradation of pollutants.

3.3. Charge transfer process

The above results confirmed that the dissolution of Ag^+ from catalysts was related to the photoactivity of the catalysts. During the photodegradation of the pollutants, two plasmon-induced electron-transfer processes occurred: the transfer between the photoexcited Ag NPs and AgBr and the transfer between 2-CP and the Ag NPs, resulting in $O_2^{\bullet-}$ and photogenerated h^+ on the Ag NPs [19,29–33]. Also, $^\bullet OH$ and $O_2^{\bullet-}$ were formed by photoexcited AgBr. The results indicated that the dissolution of Ag^+ was related to the electron transfer rate and photoreaction rate. The electron-transfer processes at the Ag–AgBr/MA-Ti1 photoanodes were followed by CV analysis under different conditions, as shown in Fig. 10. No significant current was detected at the Ag–AgBr/MA-Ti1 electrode in the dark in a N_2-saturated 0.1 M sodium sulfate aqueous solution, which indicated that no interfacial electron transfer occurred. Under visible-light irradiation, an oxidation peak appeared that was attributable to the electron transfer from photoexcited Ag NPs to the conduction band of AgBr. Moreover, the peak disappeared with the addition of phenol, suggesting an electron transfer from phenol to the Ag NPs. The concentration of dissolved Ag^+ ranged from 3 to 7 mg L^{-1} under dark conditions within a 60 min time frame, as shown in Fig. 11. Under visible-light irradiation, the concentration of dissolved Ag^+ varied from 11 to 14 mg L^{-1}, which decreased to between 3 and 7 mg L^{-1} in the presence of phenol. The results indicated that the dissolution of Ag^+ was related to interfacial charge transfer processes. The presence of phenol enhanced the interfacial electron transfer, suppressing Ag^+ dissolution. Fig. 12A

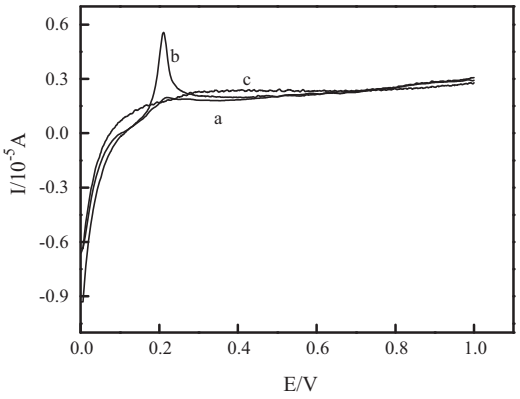

Fig. 10. The photocurrent changes at Ag–AgBr/MA-Ti1 photoanodes in an N_2-saturated 0.1 M sodium sulfate aqueous solution: (a) in dark, (b) under visible-light irradiation ($\lambda > 420$ nm) without any pollutants, and (c) under visible-light irradiation ($\lambda > 420$ nm) with 10 mg L^{-1} phenol.

shows the changes in the photocurrent at the Ag–AgBr/MA-Ti1 electrode in the presence of different electron donors. Compared with ultrapure water, the oxidation peak of the Ag NPs decreased in tap water. Components in the tap water, such as CO_3^{2-}, SO_4^{2-}, and Cl^-, acted as electron donors, which reduced the photogenerated Ag^+, thus suppressing the dissolution of Ag^+ (5 μg L^{-1} in tap water). The tested tap water in this study had CO_3^{2-}, SO_4^{2-}, and Cl^- concentrations of 21.6 mg L^{-1}, 53.2 mg L^{-1}, and 219.3 mg L^{-1}, respectively. Fig. 12B–D shows the effects of these inorganic anions on the photocurrent changes at the Ag–AgBr/MA-Ti1 electrodes in a N_2-saturated 0.1 M sodium sulfate aqueous solution. The oxidation peak gradually decreased to an indiscernible trace as the concentration of CO_3^{2-}, SO_4^{2-}, and Cl^- increased in the Na_2CO_3, Na_2SO_4, and NaCl aqueous solutions, respectively. The results confirmed that these anions could donate electrons to photogenerated h^+ in Ag NPs, forming $CO_3^{\bullet-}$, $SO_4^{\bullet-}$, and $Cl^\bullet$ radicals and enhancing the electron transfer to suppress the dissolution of Ag^+. Because the newly formed $CO_3^{\bullet-}$, $SO_4^{\bullet-}$, and $Cl^\bullet$ radicals were less active than $^\bullet OH$ and $O_2^{\bullet-}$, they could decrease the photocatalytic efficiency of Ag–AgBr/MA-Ti1. However, the photoactivity of the catalyst could increase due to the accelerating electron transfer. Overall, the photoactivity of the catalysts decreased slightly in the tap water. Given the aforementioned experimental and theoretical results, we have represented the electron transfer process during the photodegradation of pollutants in tap water as the process shown in Scheme 1.

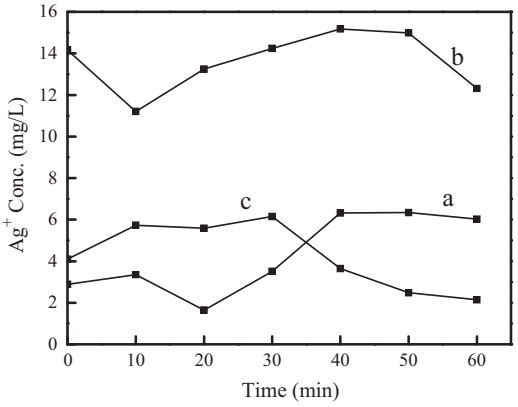

Fig. 11. The Ag^+ dissolution during the reaction from Ag–AgBr/MA-Ti1 in N_2-saturated ultrapure water (containing catalyst: 1.6 g L^{-1}; 60 mL) under visible-light irradiation ($\lambda > 420$ nm): (a) in dark and (b and c) without or with 10 mg L^{-1} phenol, respectively.

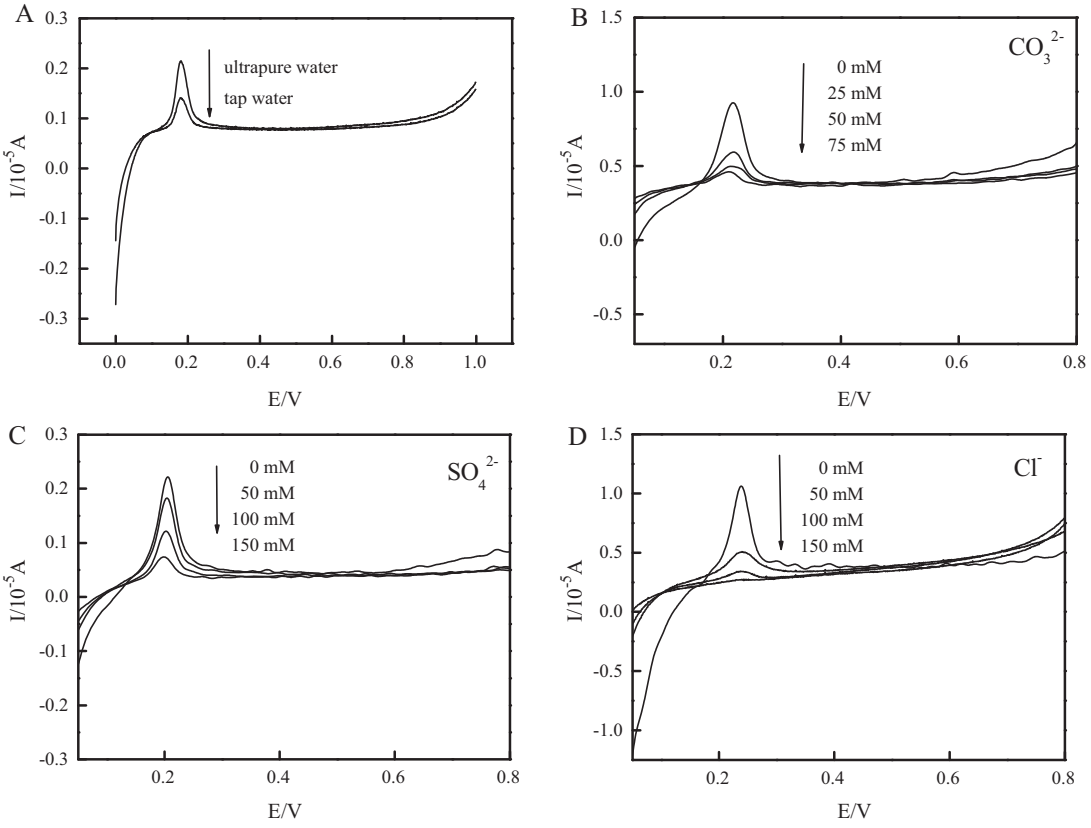

Fig. 12. Effects of different electron donors on the photocurrent changes at the Ag–AgBr/MA-Ti1 photoanode under visible-light irradiation ($\lambda > 420$ nm) in N_2-saturated 0.1 M sodium sulfate aqueous solution.

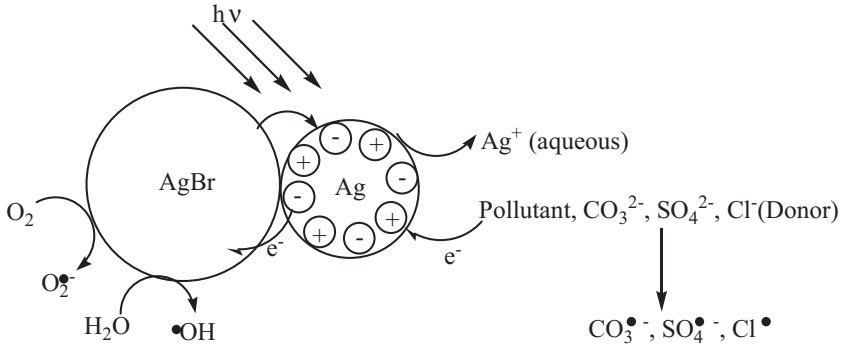

Scheme 1. Schematic of the photocatalytic reaction process and charge transfer of Ag/AgBr/MA-Ti1 under visible light illumination.

4. Conclusion

Ag–AgBr was deposited onto MA and MA-Ti1 by a deposition–precipitation method. With the increase of doped titanium in MA, the photocatalytic activity of the catalysts decreased while the Ag^+ dissolution was reduced. Although its photoactivity was slightly lower than Ag–AgBr/MA, Ag–AgBr/MA-Ti1 was considered the better catalyst for practical applications due to its reduced dissolution of Ag^+. Cyclic voltammetry analyses under a variety of experimental conditions verified that the dissolution of Ag^+ was related to charge transfer. The charge transfer resulted in the Ag^+ dissolution, which was inhibited by enhancing the electron-transfer rate. The common anions in tap water accelerated the electron transfer by trapping photogenerated h^+ on the Ag NPs, thus decreasing the release of Ag^+.

Acknowledgments

This work was supported by Project 973 (No. 2010CB933604), the NSFC (Nos. 21125731, 20807051, and 50921064) and the federal department of Chinese water control and treatment (No. 2008ZX07209-001).

References

[1] B. Kraeutler, A.J. Bard, Heterogeneous photocatalytic preparation of supported catalysts. Photodeposition of platinum on titanium dioxide powder and other substrates, J. Am. Chem. Soc. 100 (1978) 4317–4318.
[2] L. He, M.D. Musick, S.R. Nicewarner, F.G. Salinas, S.J. Benkovic, M.J. Natan, C.D. Keating, Colloidal Au-enhanced surface plasmon resonance for ultrasensitive detection of DNA hybridization, J. Am. Chem. Soc. 122 (2000) 9071–9077.

[3] T. Hirakawa, P.V. Kamat, Charge separation and catalytic activity of Ag@TiO_2 core–shell composite clusters under UV-irradiation, J. Am. Chem. Soc. 127 (2005) 3928–3934.
[4] J.H. Schattka, D.G. Shchukin, J. Jia, M. Antonietti, R.A. Caruso, Photocatalytic activities of porous titania and titania/zirconia structures formed by using a polymer gel templating technique, Chem. Mater. 14 (2002) 5103–5108.
[5] E. Szabo-Bardos, H. Czili, A. Horvath, Photocatalytic oxidation of oxalic acid enhanced by silver deposition on a TiO_2 surface, J. Photochem. Photobiol. A 154 (2003) 195–201.
[6] I.M. Arabatzis, T. Stergiopoulos, D. Andreeva, S. Kitova, S.G. Neophytides, P. Falaras, Characterization and photocatalytic activity of Au/TiO_2 thin films for azo-dye degradation, J. Catal. 220 (2003) 127–135.
[7] Y. Lin, H. Lee, Effects of TiO_2 coating dosage and operational parameters on a TiO_2/Ag photocatalysis system for decolorizing Procion red MX-5B, J. Hazard. Mater. 178 (2010) 115–122.
[8] P. Falaras, I.M. Arabatzis, T. Stergiopoulos, M.C. Bernard, Enhanced photocatalytic activity of silver modified thin-film TiO_2 photocatalyst, Int. J. Photoenergy 5 (2003) 123–130.
[9] S. Link, M.A. El-Sayed, Spectral properties and relaxation dynamics of surface plasmon electronic oscillations in gold and silver nanodots and nanorods, J. Phys. Chem. B 103 (1999) 8410–8426.
[10] M.C. Daniel, D. Astruc, Gold nanoparticles: assembly, supramolecular chemistry, quantum-size-related properties, and applications toward biology, catalysis, and nanotechnology, Chem. Rev. 104 (2004) 293–346.
[11] J.J. Mock, M. Barbic, D.R. Smith, D.A. Schults, S. Schults, Shape effects in plasmon resonance of individual colloidal silver nanoparticles, J. Chem. Phys. 116 (2002) 6755–6759.
[12] R. Jin, Y.C. Cao, E. Hao, G.S. MeÂtrauz, G.C. Schatz, C.A. Mirkin, Controlling anisotropic nanoparticle growth through plasmon excitation, Nature 425 (2003) 487–490.
[13] F. Kim, J.H. Song, P. Yang, Photochemical synthesis of gold nanorods, J. Am. Chem. Soc. 124 (2002) 14316–14317.
[14] M. GraÈtzel, Photoelectrochemical cells, Nature 414 (2001) 338–344.
[15] V. Subramanian, E. Wolf, P.V. Kamat, Semiconductor–metal composite nanostructures. To what extent do metal nanoparticles improve the photocatalytic activity of TiO_2 films, J. Phys. Chem. B 105 (2001) 11439–11446.
[16] Y. Tian, T. Tatsuma, Mechanisms and applications of plasmon-induced charge separation at TiO_2 films loaded with gold nanoparticles, J. Am. Chem. Soc. 127 (2005) 7632–7637.
[17] C. Hu, T. Peng, X. Hu, Y. Nie, X. Zhou, J. Qu, H. He, Plasmon-induced photodegradation of toxic pollutants with Ag–AgI/Al_2O_3 under visible-light irradiation, J. Am. Chem. Soc. 132 (2010) 857–862.
[18] D. Beydoun, R. Amal, G.K.C. Low, S. McEvoy, Novel photocatalyst: titania-coated magnetite. Activity and photodissolution, J. Phys. Chem. B 104 (2000) 4387–4396.
[19] X. Zhou, C. Hu, X. Hu, T. Peng, J. Qu, Plasmon-assisted degradation of toxic pollutants with Ag–AgBr/Al_2O_3 under visible-light irradiation, J. Phys. Chem. C 114 (2010) 2746–2750.
[20] P. Wang, B. Huang, X. Qin, X. Zhang, Y. Dai, J. Wei, M. Whangbo, Highly efficient visible-light plasmonic photocatalyst Ag@AgCl, Angew. Chem. Int. Ed. 47 (2008) 7931–7936.
[21] P. Wang, B. Huang, X. Zhang, X. Qin, J. Hao, Y. Dai, Z. Wang, J. Wei, J. Zhan, S. Wang, J. Wang, M. Whangbo, Highly efficient visible-light plasmonic photocatalyst Ag@AgBr, Chem. Eur. J. 15 (2009) 1821–1824.
[22] C. Hu, Y. Lan, J. Qu, X. Hu, A. Wang, Ag/AgBr/TiO_2 visible light photocatalyst for destruction of azodyes and bacteria, J. Phys. Chem. B 110 (2006) 4066–4072.
[23] B. Xu, T. Xiao, Z. Yan, X. Sun, J. Sloan, L. González-Cortés, F. Alshahrani, M.L.H. Green, Synthesis of mesoporous alumina with highly thermal stability using glucose template in aqueous system, Micropor. Mesopor. Mater. 91 (2006) 293–295.
[24] K. Shimizu, J. Shibata, H. Yoshida, A. Satsumal, T. Hattori, Silver–alumina catalysts for selective reduction of NO by higher hydrocarbons: structure of active sites and reaction mechanism, Appl. Catal. B 30 (2001) 151–162.
[25] A.A. Christy, O.M. Kvalheim, R.A. Velapoldi, Quantitative analysis in diffuse reflectance spectrometry: a modified Kubelka–Munk equation, Vib. Spectrosc. 9 (1995) 19–27.
[26] L. Zhang, C. Zhang, H. He, The role of silver species in Ag/Al_2O_3 catalysts for the selective catalytic oxidation of ammonia to nitrogen, J. Catal. 261 (2009) 101–109.
[27] A. Ledo, F. Martínez, M.A. López-Quintela, J. Rivas, Synthesis of Ag clusters in microemulsions: a time-resolved UV–vis and fluorescence spectroscopy study, Physica B 398 (2007) 273–277.
[28] J. Han, W. Qiu, W. Gao, Potential dissolution and photo-dissolution of ZnO thin films, J. Hazard. Mater. 178 (2010) 115–122.
[29] C. An, S. Peng, Y. Sun, Facile synthesis of sunlight-driven AgCl:Ag plasmonic nanophotocatalyst, Adv. Mater. 22 (2010) 2570–2574.
[30] M. Zhu, P. Chen, M. Liu, Graphene oxide enwrapped Ag/AgX (X = Br, Cl) nanocomposite as a highly efficient visible-light plasmonic photocatalyst, ACS Nano 5 (2011) 4529–4536.
[31] Y. Zhanga, Z. Tanga, X. Fua, Y. Xu, Nanocomposite of Ag–AgBr-TiO_2 as a photoactive and durable catalyst for degradation of volatile organic compounds in the gas phase, Appl. Catal. B 106 (2011) 445–452.
[32] H. Cheng, B. Huang, P. Wang, Z. Wang, Z. Lou, J. Wang, X. Qin, X. Zhang, Y. Dai, In situ ion exchange synthesis of the novel Ag/AgBr/BiOBr hybrid with highly efficient decontamination of pollutants, Chem. Commun. 47 (2011) 7054–7056.
[33] L. Kuai, B. Geng, X. Chen, Y. Zhao, Y. Luo, Facile subsequently light-induced route to highly efficient and stable sunlight-driven Ag–AgBr plasmonic photocatalyst, Langmuir 26 (2010) 18723–18727.